

AIRCRAFT OBSERVATIONS OF THE MEAN AND TURBULENT STRUCTURE OF A SHALLOW BOUNDARY LAYER OVER THE PERSIAN GULF

IAN M. BROOKS and DAVID P. ROGERS

Scripps Institution of Oceanography, La Jolla, California, U.S.A.

(Received in final form 8 November 1999)

Abstract. Stable internal boundary layers form when warm air is advected over a cooler surface, a common occurrence in coastal areas. The internal boundary layer deepens with distance along-wind, eventually reaching equilibrium with the surface and becoming a fully developed marine boundary layer. We present observations of the late stages of internal boundary-layer evolution made by the U.K. Meteorological Office's C-130 Hercules research aircraft over the Persian Gulf in April 1996. Northwesterly winds brought warm dry air from the surrounding desert landmass across the cooler waters of the Gulf. Loss of heat to the surface resulted in the formation of a shallow, stable internal boundary layer downwind of the coast. The aircraft measurements were made several hundred kilometres downwind, by which point the original deep convective boundary layer had been eroded away and the internal boundary layer was well developed, effectively a new marine atmospheric boundary layer. Throughout most of its depth the boundary layer was statically stable and a downward heat flux of approximately 15 W m^{-2} was observed; however, an exceptionally strong latent heat flux, in excess of 250 W m^{-2} near the surface, was sufficient to overcome the downwards heat flux and maintain weak buoyant convection in the lower 30–50% of the boundary layer.

Scaling of boundary-layer turbulence statistics using local similarity theory produces results in agreement with previous studies. Because of the strong humidity contribution to the buoyancy flux, however, care is required with the definition of the similarity scales. It is usual for either the sensible heat or buoyancy flux to be used in the definitions of both the temperature and length scales; the latter being used over water where humidity plays a significant role in determining stability. In the present case we find that while the buoyancy flux is appropriate in the definition of the length scale, the temperature scale must be defined in terms of the sensible heat flux.

Keywords: Internal boundary layer, Local similarity.

1. Introduction

Stable boundary layers over the oceans have received relatively little attention compared to convective conditions. They present a particular challenge for observational studies due to low turbulence levels, frequent horizontal heterogeneity, and the lack of a well-defined, universally applicable theoretical framework to describe their structure (Nappo and Bach, 1997). An increasing need to understand small-scale boundary-layer and air-sea interaction processes in coastal regions (Rogers, 1995) where stable boundary layers and internal boundary layers are frequent and sometimes persistent features, is focussing increased attention in this area.



Boundary-Layer Meteorology **95**: 189–210, 2000.

© 2000 Kluwer Academic Publishers. Printed in the Netherlands.

An internal boundary layer (IBL) is formed when air is advected across a discontinuity in surface conditions such as roughness or temperature. Such layers are a common feature of coastal environments, where large changes in surface roughness and the fluxes of heat and moisture can occur at the land-sea interface. Stable internal boundary layers have received less attention than the unstable case (Garratt, 1987), but are important for a number of reasons. They can strongly affect the interaction of the surface with the boundary layer (BL) as a whole (Friehe et al., 1991; Koracin and Rogers, 1990; Rogers et al., 1995a,b) and are of particular importance to the problem of radar ducting, an issue which prompted some of the earliest observational studies (Craig, 1946; Emmons, 1947) and continues to focus attention in this area (Mulhearn, 1981; Brooks et al., 1999). There have been, until recently, few observational studies of the stable IBL (see Garratt, 1990, for a review). Mulhearn (1981) noted that the best measurements available to him were some 35 years old – those of Craig (1946). More recently a number of experimental and theoretical studies have focused on the stable IBL. Most have considered the case of offshore flow over the sea (Garratt, 1987; Garratt and Ryan, 1989; Melas, 1989; Hsu, 1993; Rogers et al., 1995a,b; Smedman et al., 1997), others have considered advection across a sea-surface temperature front (Friehe et al., 1991; Rogers, 1989; Koracin and Rogers, 1990).

The general evolution of the stable IBL is now well documented. When warm air is advected over the cooler sea, heat loss to the surface cools the lowest part of the BL resulting in a shallow stable layer – the internal boundary layer. The stability inhibits vertical mixing between the IBL and the air above so that the two layers evolve almost independently. Decoupling of the upper boundary layer from surface friction allows acceleration of the flow above the IBL and the formation of a low-level wind speed jet. The increased shear at the top of the stable layer mechanically forces turbulent mixing at the boundary, entraining air into the IBL and deepening the layer. The stable IBL evolves continuously, though slowly, with distance downstream, eventually becoming the new marine atmospheric boundary layer as the remains of the old BL erode. It may, however, take several hundred kilometres before it reaches equilibrium with the surface, much further than for the unstable case (Garratt, 1990). While the heat flux is by definition negative (downwards) in such cases, moisture fluxes at the surface depend upon the initial humidity of the air and the air-sea temperature difference. Garratt and Ryan (1989) observed positive (upwards) moisture fluxes leading to an increase in humidity within the IBL, while Rogers et al. (1995a) observed the humidity mixing ratio to decrease along wind near the surface, implying a negative flux and loss of moisture to the surface.

Our understanding of turbulent processes under stable conditions has lagged behind that for neutral and unstable boundary layers and there remain many unanswered questions (Nappo and Bach, 1997). Measurements within stable layers can be more difficult than under convective conditions due to the low intensity of turbulence and its sometimes intermittent nature. Stable boundary layers can be

horizontally highly variable, thus measurements at one location are not necessarily representative of the BL as a whole. Studies are further complicated by a variety of forcing processes: radiative cooling, heat loss to a cooler surface, interaction of turbulence and gravity waves, and shear generation of turbulence both at the surface and the top of the stable layer. Uncertainties in the parameterisation of surface fluxes lead to poor performance by numerical models of stable layers (Nappo and Bach, 1997). No entirely satisfactory similarity theory exists for the stable BL. Studies of radiatively driven night-time boundary layers over land have led to the development of a local similarity theory (Nieuwstadt, 1984; Sorbjan, 1986,1987). This follows the form of Monin–Obukhov surface similarity theory, but relates the non-dimensional fields to local scales rather than to scales based on surface fluxes. Local similarity has been successfully applied to a variety of situations under both stable and unstable conditions (Sorbjan, 1986; Shao and Hacker, 1990) but there remains a question as to whether it can be universally applied within stable boundary layers (Nappo and Bach, 1997).

This study presents observations made by the C-130 Hercules research aircraft operated by the U.K. Meteorological Office's Meteorological Research Flight (MRF) over the Persian Gulf in late April 1996. The measurements were made in support of a US Navy Ship Antisubmarine warfare Readiness/Effectiveness Measuring exercise (SHAREM-115).

The Persian Gulf is entirely surrounded by desert landmass. The boundary layer above such an enclosed sea will rarely be free of the effects of the surrounding land since advective effects will influence the BL regardless of wind direction (Smedman et al., 1997). Throughout this study the prevailing winds were northwesterly resulting in an over-water fetch of several hundred kilometres to the measurement region in the central Gulf. These observations are thus made at a much later stage of IBL evolution than those of most of the previous studies cited above. At the measurement location the boundary layer was found to be a very well-developed internal boundary layer – effectively at the stage of having become the boundary layer proper rather than a part of the deeper pre-existing boundary layer.

2. Measurements

The MRF C-130 Hercules is a heavily instrumented atmospheric research aircraft. Its standard suite of instruments measures a wide range of meteorological, dynamic, radiative, and microphysical variables. The three wind components are derived from a pitot-static pressure system and two wind vanes, or gust probes, all situated near the tip of a 7-m nose boom in the undisturbed air ahead of the aircraft. Aircraft motions are monitored by an inertial navigation unit, which is corrected for long period drift and Schuler oscillations by comparison with data from a global positioning system (GPS). Temperature is measured by a Rosemount platinum-resistance thermometer. Dew point temperature and total water mixing

ratio are measured by a Lyman- α absorption hygrometer, which is continuously calibrated against a General Eastern cooled mirror hygrometer when in clear air. The sea surface temperature (SST) is measured radiometrically by a Heimann infrared radiometer. All parameters are sampled at 32 Hz except the humidity which is sampled at 64 Hz. Turbulence properties are calculated from the 32 Hz data, mean conditions are determined from 1 second averaged data. The Rosemount temperature probe is known to suffer from a poor response at frequencies greater than 0.1 Hz due to the thermal mass of the sensing element and shroud. The time constants are known from laboratory calibration (Nicholls, 1982) and much of the high frequency signal may be recovered by means of a digital filter (McCarthy, 1973). The filtered temperature has a unity frequency response up to 1 Hz, above this the response falls off rapidly and drops below the unfiltered response at frequencies above 7 Hz, corresponding to spatial scales of ~ 14 m at a nominal airspeed of 100 m s^{-1} . The loss of sensitivity at these highest frequencies does not present a serious cause for concern since the contribution to the heat flux is generally negligible at such small scales.

A total of five research flights were made between April 23 and 29. Flying times and locations were restricted by the requirement to fit in with the operations of the naval exercise. We present data from the flight on April 28. The sampling strategy was designed to characterise the vertical structure and horizontal variability of the boundary layer; the flight track is shown in Figure 1. Stacks of straight and level flight legs, oriented perpendicular to the mean wind, were flown at the northwestern (upwind) and southeastern (downwind) extremes of the operational area. These were intended to characterise the turbulent structure of the boundary layer. A series of sawtooth profiles along the same ground-tracks and extending from 15 m above the surface to just above the BL inversion measured the mean vertical structure and its variability. Further sawtooth profiles were made along-wind to determine the along-wind variability and evolution of the BL structure. Horizontal flight legs oriented along-wind were made where time allowed, and occasional deeper profiles, extending up to 1000 m, were made to determine the general structure of the lower atmosphere. Measurements of the initial BL state at the coast, prior to advection over the Gulf are obtained from the standard synoptic upper air soundings made at Kuwait International Airport (KIA), several hundred kilometres upwind.

3. Results

Synoptic conditions on April 28 were dominated by a region of high pressure over Turkey with a secondary high over Saudi Arabia resulting in a winter Shamal – a period of high, generally northerly winds (Perrone, 1979). The Shamal started on April 26 and persisted through the end of the field program on April 29. It was accompanied by mesoscale subsidence over the Gulf. Wind speed and direction

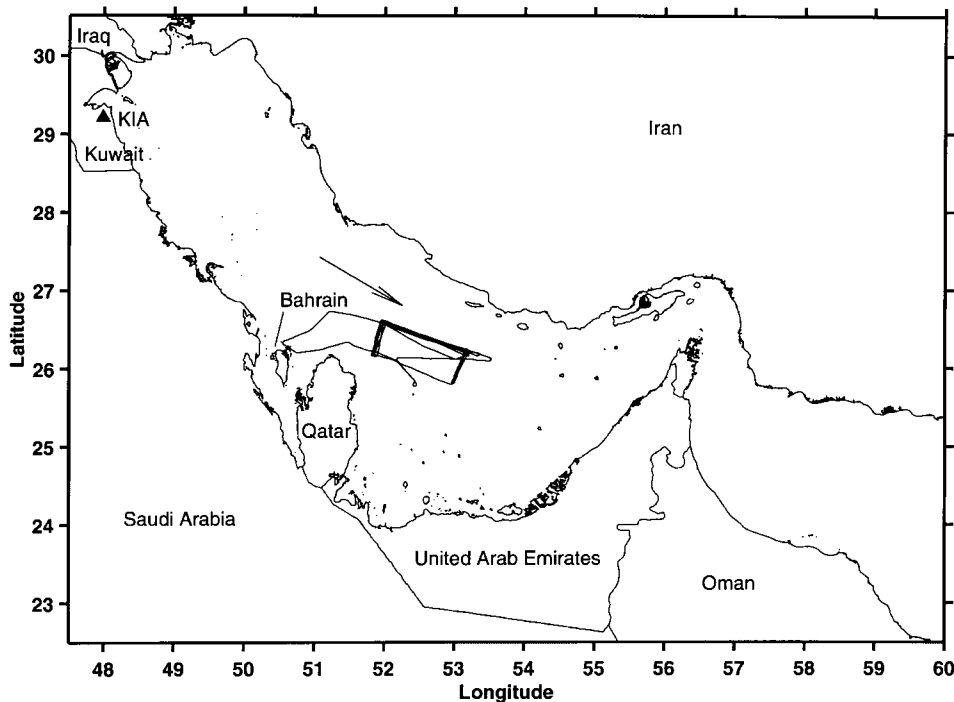


Figure 1. Map of the Persian Gulf showing the aircraft flight track from April 28 and the location of Kuwait International Airport (KIA). The mean BL wind direction is indicated by the large arrow.

remained very uniform throughout this period; wind speed peaked at $22\text{--}23\text{ m s}^{-1}$ just above the boundary-layer inversion and the direction was from between northwest and north-northwest, almost directly down the long axis of the Persian Gulf. As warm air is advected from the desert landmass over the cooler waters of the Gulf, heat loss to the surface will result in the formation of a stable internal boundary layer. Our observations were made several hundred kilometres downwind of the coast where the IBL has evolved to the stage where it has become a new marine boundary layer.

Figure 2 shows profiles of virtual potential temperature, humidity, and wind speed and direction from synoptic soundings at Kuwait International Airport (KIA) at 0000 and 1200 UTC on April 28 and from aircraft profiles at the downwind end of the operational area at 0350 and upwind at 1010 UTC (throughout this paper references to *upwind* and *downwind* measurements refer to the region of aircraft measurements only; measurements far upwind at the coast are noted as such. Local time is UTC-3 hours). Note that the profiles do not represent the same air mass, only the general changes in conditions between the coast and central Gulf. Also, the change in wind speed with altitude means that the aircraft profiles do not represent a column of air that crossed the coast at the same time. Given the wind speeds near the surface and at the peak of the wind speed jet, we can

estimate transit times from the coast. Thus the downwind profile at 0350 UTC represents air that crossed the coast between approximately 1000 and 1900 UTC on April 27 and having properties very similar to those shown in the 1200 UTC profile from KIA. The upwind profile at 1010 UTC represents air that left land between 1900 UTC on April 27 and 0300 UTC on April 28 and having properties closer to the 0000 sounding at KIA. Sunrise and sunset are at approximately 0300 and 1500 UTC respectively. The daytime boundary layer at KIA is approximately 2000 m deep, well mixed and convective. The humidity is low, with a mixing ratio of about 2.5 g kg^{-1} . At night radiative cooling causes a decrease in near surface temperature. The remains of the well-mixed layer from the previous day are still clearly visible in the θ_v profile. The wind speed and direction profiles show the wind to remain relatively unchanged throughout most of the lowest 2000 m; near the surface however, wind speed and direction show a strong dependence on land/sea breeze effects. The aircraft profiles show a much shallower BL than that overland, approximately 250–300 m deep. The near surface temperature has increased/decreased towards the surface temperature, and the humidity mixing-ratio has increased/dramatically to approximately 10 g kg^{-1} . The humidity profiles have a very rounded appearance indicating that mixing is poor within the layer and the sharp drop in humidity across the inversion shows that there is little or no transport out of the surface layer. The similarity between the aircraft profiles suggests that the BL air is approaching equilibrium with the surface, becoming a marine boundary layer with properties to some degree independent of those of the air crossing the coast. The most significant difference between the profiles is that in temperature – this is due primarily to subsidence warming as discussed below – and local variations in the sea surface temperature.

Modification of the boundary-layer air by the surface can be illustrated by means of a conserved variable mixing diagram. Total water mixing ratio and equivalent potential temperature are conserved quantities for an air mass under adiabatic conditions. The properties of a parcel of air are represented by a point on the mixing diagram. The diagram fulfils the properties of mixtures almost exactly so that a mixture of two air parcels results in a point that lies on a straight line joining the initial air masses; the relative distance from the initial points being proportional to the masses in the mixture. The properties of the surface can be represented by a point at the surface temperature and at saturated humidity. Figure 3 shows a mixing diagram for two profiles, at the upwind and downwind ends of the region along with the co-located surface values. Points within the BL are stretched out along a mixing line between those representing the air above the BL, and those in equilibrium with the surface. The approximate altitude of the points in each profile is indicated. Using the properties of mixtures we can infer that at 300 m in the upwind profile the modification of the air mass is equivalent to the mixing of approximately 85% continental air and 15% air with surface properties. At 100 m the mixture is close to 60% continental air and 40% surface air. The extent of modification is slightly higher for the downwind profile, but the low overall mixing

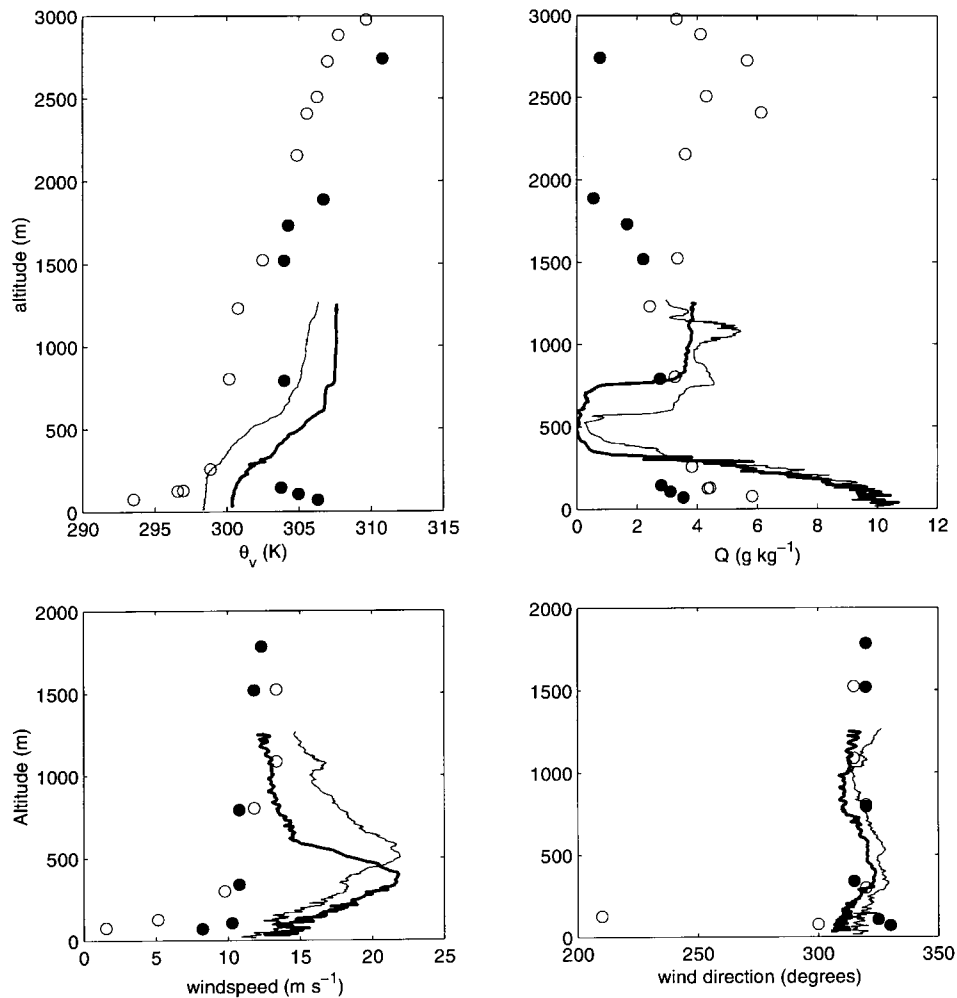


Figure 2. Profiles of virtual potential temperature, humidity mixing ratio, wind speed and direction from Kuwait International airport ($29^{\circ}13' \text{ N}$, $47^{\circ}59' \text{ E}$) at 0000 UTC (open circles) and 1200 UTC (solid circles), and aircraft profiles at $26^{\circ}12' \text{ N}$, $53^{\circ}19' \text{ E}$ at 0350 UCT (downwind, thick line) and $26^{\circ}07' \text{ N}$, $52^{\circ}07' \text{ E}$ at 1010 UTC (upwind, thin line).

ratios and relatively small change in properties over a distance of 125 km reveals the poor mixing within the BL as a whole. The adjustment of the BL to slowly changing surface conditions is seen in the offset between values within the BL; note that the values above the BL are unaffected by the changes at the surface.

The IBL formed at the coast is now well developed and has replaced the original deep convective BL, of which little sign remains in the aircraft profile. The BL has not yet adjusted fully to the surface conditions, and significant evolution along wind is observed within the measurement area. Figure 4 shows two profiles of potential temperature and total water mixing ratio made at the upwind and downwind ends of

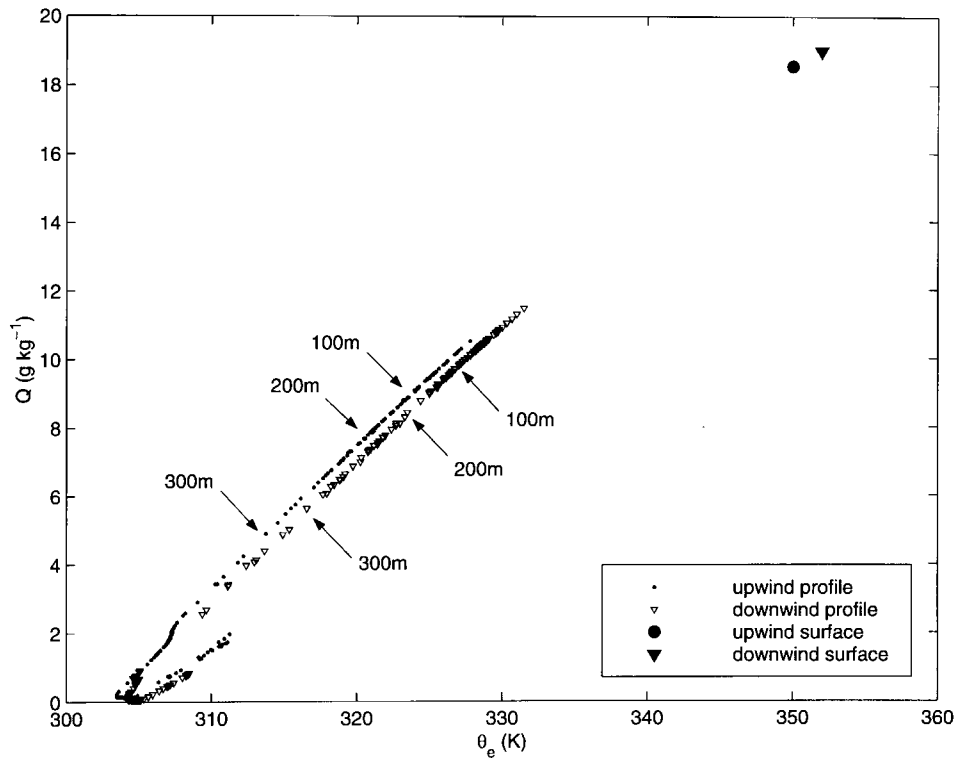


Figure 3. Conserved variable mixing diagram for equivalent potential temperature and total water mixing ratio for an aircraft profiles at $26^{\circ}34' \text{ N}$, $52^{\circ}02' \text{ E}$, and 0630 UTC (upwind, small circles), and $26^{\circ}12' \text{ N}$, $53^{\circ}10' \text{ E}$, and 0650 UTC (downwind, open triangles) with the co-located surface properties (large circles and solid triangles respectively). The approximate altitude of the points in each profile are indicated by arrows.

the region. There is a general warming of approximately 3 K throughout the lower atmosphere. Warming due to changes in radiative heating during the day may be discounted since repeated measurements at the same location separated by several hours gave almost identical results. The warming is likely due to the mesoscale subsidence over the Gulf, associated with the shamal conditions. Subsidence also results in a gradual decrease in BL depth with distance along-wind, also evident in these profiles. The difference in temperature between the two profiles within the boundary layer is only half that for the air above; the general warming being offset by a heat loss to the surface of approximately 15 W m^{-2} . The total water mixing-ratio within the lower BL increases by approximately 1.5 g kg^{-1} in the 150 km between the profiles. This is consistent with a measured latent heat flux of the order of 250 W m^{-2} at the upwind end of the region, falling to approximately 200 W m^{-2} downwind.

Profiles of wind stress, sensible and latent heat fluxes, and buoyancy flux for the two stacks of level runs on April 28 are shown in Figure 5. Sensible heat fluxes

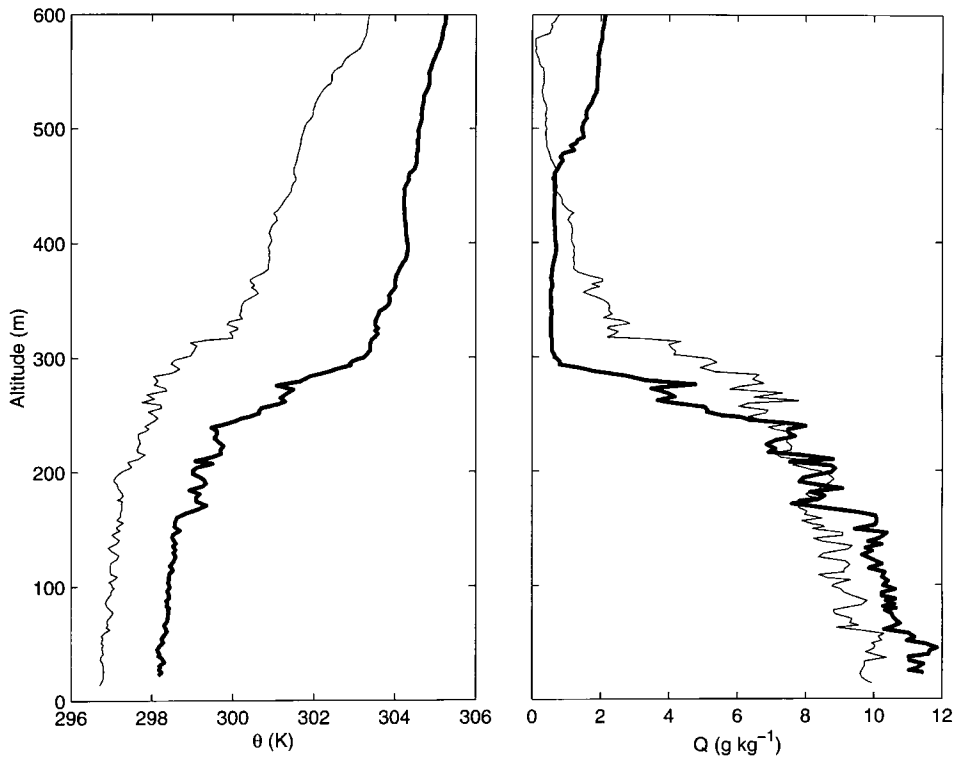


Figure 4. Profiles of potential temperature and total water mixing ratio on April 28 at the following locations and times: upwind (thin line), $26^{\circ}34'$ N, $52^{\circ}03'$ E, 0853 UTC; downwind (thick line), $26^{\circ}08'$ N, $53^{\circ}29'$ E, 0915 UTC.

are relatively uniform at approximately -15 W m^{-2} throughout the BL at both locations. Latent heat fluxes are very large near the surface, $200\text{--}250 \text{ W m}^{-2}$, decreasing with altitude to near zero above the inversion. The fluxes at the uppermost level downwind are due to variability at scales $>2 \text{ km}$ rather than turbulent transport. There is a decrease in latent heat flux of about 50 W m^{-2} between the upwind and downwind 30 m flight legs, due to the decreasing vertical humidity gradient as the BL moistens. The positive buoyancy flux in the lower BL results from the exceptionally large moisture flux, which overcomes the stabilising influence of the downwards sensible heat flux. Mulhearn (1981) noted the possibility of buoyancy driven by the humidity flux when warm, dry air is advected over cooler water, provided that the air was very dry and the initial air-sea temperature difference not too great. We are not aware, however, of any previous measurements of such a situation in the literature. The buoyancy flux may be partitioned into contributions from the sensible heat and humidity fluxes as

$$\overline{w'\theta'_v} = \overline{w'\theta'}(1 + 0.61\overline{Q}) + 0.61\overline{\theta}(w'Q') \quad (1)$$

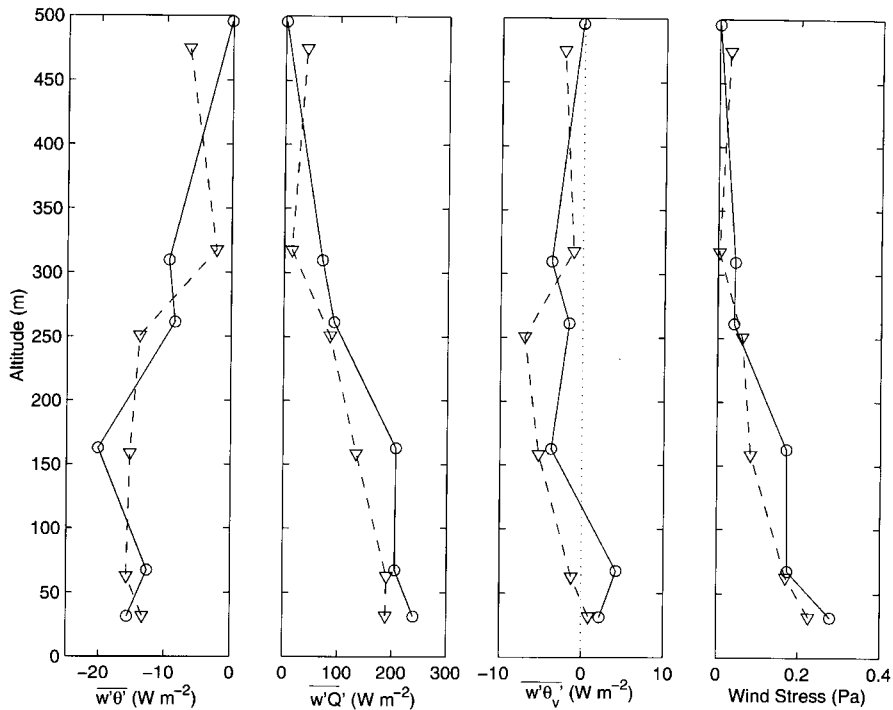


Figure 5. Profiles of sensible and latent heat flux, and buoyancy flux at the upwind (circles) and downwind (triangles) ends of the measurement area on April 28.

where Q is the humidity mixing ratio in kg/kg, θ is the potential temperature and w the vertical velocity (Stull, 1988, p. 146). Primed terms are perturbations from the mean, and an overbar indicates an average – ideally an ensemble average, in practice a spatial average over one flight leg. Figure 6 shows ogive curves for the heat and humidity flux contributions to the buoyancy flux, and the total buoyancy flux for the upwind stack. The ogives are the running integral of the cospectral density (Friehe et al., 1991; Rogers et al. 1995), so that any given point represents the cumulative contribution to the flux from all higher frequencies. Provided the turbulence is stationary the total flux is approached asymptotically at low frequencies. A nominal airspeed of 100 m s^{-1} allows the frequency scale to be transformed to a spatial scale, so that $1 \text{ Hz} = 1 \text{ km}$, $10 \text{ Hz} = 100 \text{ m}$. The sensible and latent heat contributions to the buoyancy flux are seen to be almost equal in magnitude but of opposite sign, the total buoyancy flux is determined by the small imbalance. Near the surface the strong moisture flux dominates and weak convection is possible. This extends through less than half of the BL depth. The humidity flux decreases with altitude and above about 100–150 m is insufficient to overcome the downward heat flux, which remains relatively constant with altitude. Although the positive buoyancy flux represents a dramatic extreme in terms of the relative contributions

of heat and moisture fluxes to the forcing, it contributes little to the overall forcing of the BL, which remains dominated by shear forcing. The buoyant forcing contribution to turbulent kinetic energy budget ($\overline{w'\theta'_v}(g/\theta_v)$) is of the order of just 2% that of the shear contribution ($-\overline{w'u'}(\partial\overline{U}/\partial z)$) at 30 m at the upwind end of the region, falling to 1.5% downwind. We can infer a larger contribution at locations closer to the coast. Similar weak buoyancy forcing near the surface was observed on all but one of the flights during this field program. Note that the ogives for the sensible heat contribution show an upwards, counter-gradient, transport of heat at frequencies greater than ~ 2 Hz (spatial scales less than ~ 50 m). A similar counter-gradient heat flux at small scales was observed within a stable internal boundary layer by Rogers et al. (1995). It is attributed to the breakdown of larger scale eddies which transport warm air down from higher within the BL, and the return of fluid elements towards their level of neutral buoyancy.

4. Similarity

The turbulence conditions observed during SHAREM-115 present an interesting situation. The downwards heat flux maintains stable stratification throughout the larger part of the BL depth; a strong surface moisture flux, however, overcomes this and drives weak buoyant convection in the lowest part of the layer. A balance between the surface heat loss and a general warming due to subsidence maintains a near constant value of the heat flux over a range of at least 150 km along wind. The moisture flux decreases continuously along wind as the humidity increases thus the height over which a positive buoyancy flux is maintained decreases along wind. Local similarity theory provides an attractive approach to scaling such a BL. It was first introduced by Nieuwstadt (1984) for stable conditions and further developed by Sorbjan (1986, 1987) for both stable and unstable conditions. Shao and Hacker (1990) have shown that it can be applied to horizontally heterogeneous environments, at least under conditions where the local forcing processes are more important than the effects of advection.

Local similarity theory extends Monin–Obukhov (MO) surface-layer similarity theory above the surface layer. The local similarity scaling parameters are analogous to the MO scales, but are derived from the *local* values of turbulent quantities at a given level rather than from surface values. Within the surface layer the local and MO scales are identical. The local velocity, temperature, humidity, and length scales can be defined as

$$\begin{aligned}
 u_L(z) &= [\overline{w'u'^2} + \overline{w'v'^2}]^{1/4} \\
 \theta_L(z) &= -\overline{w'\theta'}/u_L \\
 Q_L(z) &= -\overline{w'Q'}/u_L \\
 L_L(z) &= -u_L^3/[\kappa\beta\overline{w'\theta'}] \\
 &= u_L^2/[\kappa\beta\theta_L(z)]
 \end{aligned} \tag{2}$$

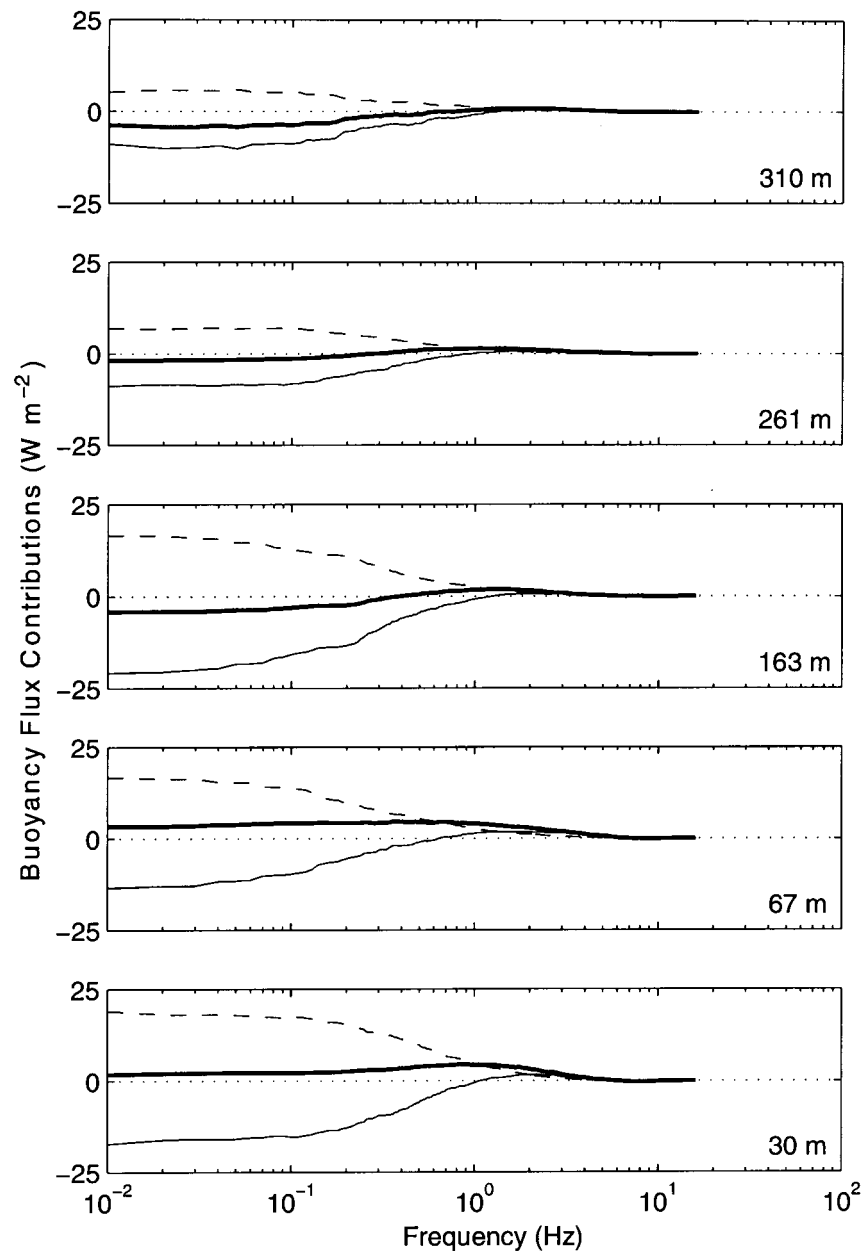


Figure 6. Ogive curves for the sensible heat (thin line), latent heat (dashed line) contributions, and total (thick line) buoyancy fluxes for the upwind stack of turbulence runs on April 28.

where κ is the von Kármán constant, here taken to be 0.4, and $\beta = g/\theta_v$ is the buoyancy parameter. Scales for other scalar variables are defined in the same manner as the temperature and humidity scales. The factor of -1 in the temperature, humidity, and length scales is included by convention. In the case of the length scale it provides consistency with the sign of the Richardson number – negative for convective conditions, positive for stable; other scales are defined to provide a consistent or convenient sign for normalised quantities. Note that the scales as defined here, and the analogous MO scales, were derived and tested using measurements made over land where humidity effects are generally small. Over water humidity makes a significant contribution to buoyancy, as demonstrated in the previous section, and potential temperature is replaced by virtual potential temperature wherever buoyancy effects are important. Thus the temperature and length scales in (2) are commonly redefined as

$$\begin{aligned}\theta_L(z) &= -\overline{w'\theta'_v}/u_L \\ L_L(z) &= -u_L^3/[\kappa\beta\overline{w'\theta'_v}] \\ &= u_L^2/[\kappa\beta\theta_L(z)].\end{aligned}\quad (3)$$

This change is essential if L_L is to correctly represent the relationship between shear and buoyant forcing. The change to the definition of θ_L has become customary and maintains the relationship with L_L established over land. Where humidity effects are small, θ_v approaches θ and the scales in (3) become identical with the definitions in (2). The definitions in (3) are those generally given in standard texts (Stull, 1988; Garratt, 1992). We will see, however, that the definition of θ_L in (3) is not generally applicable. We should note that it is also possible to define the local scales in terms of a convective velocity scale (Sorbjan, 1986; Shao and Hacker, 1990); however, this is appropriate only for unstable conditions. The scales defined above are more easily applied to both stable and unstable conditions, failing only when the wind stress approaches zero causing θ_L and Q_L to become undefined.

Table I summarises the local scaling parameters for the two stacks of turbulence runs made on April 28; only those flight legs within the BL are included. Also tabulated are scaled values of the standard deviations of temperature, σ_θ , and humidity, σ_Q , the along- and across-stream wind components, σ_u and σ_v , vertical velocity, σ_w , and $\sigma_U = (\sigma_u^2 + \sigma_v^2)^{0.5}$. The temperature scale is given for both of the definitions above to demonstrate the problems resulting from the use of (3). The layer depth h is taken to be 300 m for the upwind stack, 270 m for the downwind stack. These must be considered approximate values only since the BL depth was observed to vary by several tens of meters and is not necessarily the same for each flight leg in the stack, or even for the entire length of a given flight leg. The lowest level flight legs, at approximately 30 m, are thus at the upper limits of the surface layer, which is assumed to be approximately 10% of the overall BL depth. The range of mean values found in previous studies for stable conditions (Nieuwstadt, 1984; Sorbjan, 1986, 1987; Shao and Hacker, 1990; Tjernström and Smedman, 1993; Rogers et al.,

1995) are given below for comparison. The value for σ_Q/Q_L is an estimated mean value from Shao and Hacker (1990, Figure 8), one of very few studies to apply local scaling to humidity measurements. It should be considered an approximation only due to the high degree of scatter in their observations, which were made in a horizontally heterogeneous coastal environment. Individual estimates ranged from 0.7 to 5.7 with a standard deviation of 1.2:

$$\begin{aligned}
 \sigma_u/u_L &\approx 2.0, 2.4 \\
 \sigma_v/u_L &\approx 2.0 \\
 \sigma_U/u_L &\approx 2.0, 3.1 \\
 \sigma_w/u_L &\approx 1.4\text{--}2.0 \\
 \sigma_\theta/\theta_L &\approx 2.4\text{--}4.7 \\
 \sigma_Q/Q_L &\approx 3.0.
 \end{aligned} \tag{4}$$

We will consider first the definition of the temperature scale. Table I includes values of θ_L and the scaled standard deviation of θ calculated both from (2) in terms of the sensible heat flux (bold type) and from (3) in terms of the buoyancy flux (italic type). The latter definition clearly is not successful; values of the scaled temperature deviation range from -49 to 34 . The definition from (2), however, does appear successful with all scaled values being close to 3, well within the range observed by previous studies. The definition in (3) fails because of the large humidity contribution to the buoyancy flux. We can use (1) to determine the error arising from the use of the buoyancy flux instead of the heat flux in the definition of θ_L ,

$$\text{fractional error} = \frac{\overline{w'\theta'_v}}{\overline{w'\theta'}} - 1 = 0.61 \left(\overline{Q} + \overline{\theta} \cdot \frac{\overline{w'Q'}}{\overline{w'\theta'}} \right). \tag{5}$$

Figure 7 shows the ratio of buoyancy flux to sensible heat fluxes as a function of the ratio of latent to sensible heat fluxes calculated for the mean conditions observed: $\overline{\theta} \approx 300$ K, and $\overline{Q} \approx 0.01$ kg kg⁻¹. The measured values for each run are plotted and the fractional error in θ_L indicated. Where the magnitudes of the latent and sensible heat fluxes are similar, there will be little difference between the definitions of θ_L ; where they differ significantly, as here, there will be a substantial difference in value between the two definitions. Even so, if the ratio of fluxes remains constant then both definitions should successfully scale the temperature, although with an offset between the resultant values of scaled temperature. Temperature scaling fails for (3) when the ratio of the fluxes changes significantly as in the present results. For the remainder of the discussion of local scaling we will use θ_L as defined in (2).

The values of Q_L all lie with the narrow range of -0.13 to -0.19 , and the majority of the scaled values of σ_Q lie within the range -2.07 to -2.66 . Note that

TABLE I

Local similarity scaling variables and scaled standard deviations for the upwind (first five rows) and downwind (last four rows) stacks of turbulence runs on April 28. The temperature scale is given for both definitions $\overline{w'\theta'}/u_L$ (italics) and $\overline{w'\theta'}/u_L$ (bold). L_L is defined using the buoyancy flux as in (3). $\sigma_U = (\sigma_u^2 + \sigma_v^2)^{0.5}$.

z (m)	L_L (m)	z/L_L	u_L (m s ⁻¹)	θ_L (10 ⁻³ K)	Q_L (g kg ⁻¹)	σ_u/u_L	σ_v/u_L	σ_U/u_L	σ_w/u_L	σ_θ/θ_L	σ_Q/Q_L		
31	-4643	-0.007	0.49	-3.87	27.32	-0.17	2.58	1.90	3.20	1.17	-24.87	3.52	-2.46
67	-1205	-0.056	0.38	-9.23	28.02	-0.19	2.72	2.32	3.58	1.32	-9.54	3.18	-2.07
162	1328	0.122	0.38	8.39	45.14	-0.19	2.46	2.23	3.33	1.19	13.76	2.56	-2.35
261	349	0.746	0.18	7.59	39.50	-0.17	3.47	2.39	4.85	1.83	16.07	3.09	-2.36
309	166	1.861	0.19	17.11	42.54	-0.13	2.98	2.93	4.18	1.38	11.87	4.78	-4.17
32	-8823	-0.004	0.44	-1.67	25.93	-0.15	2.62	1.76	3.16	1.11	-49.7	3.20	-2.46
63	3993	0.016	0.38	2.77	35.38	-0.18	2.45	1.91	3.11	1.25	34.3	2.68	-2.16
159	317	0.502	0.27	17.11	49.56	-0.17	2.98	2.55	3.92	1.33	9.69	3.35	-2.66
251	153	1.644	0.23	26.61	52.49	-0.13	3.11	2.76	4.15	1.34	11.8	5.98	-5.64

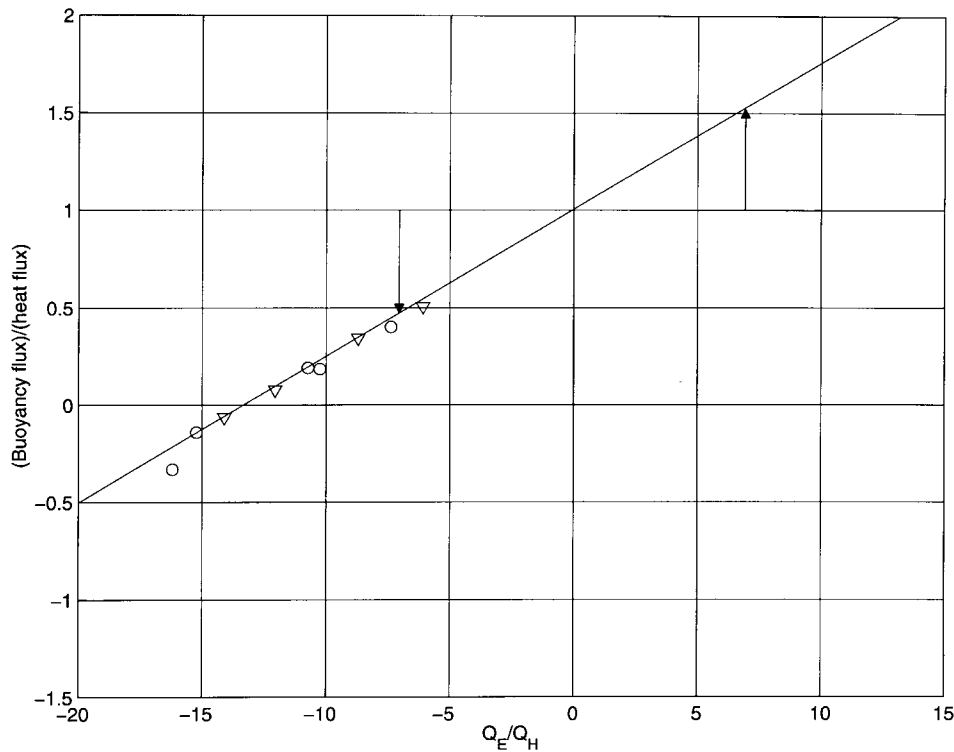


Figure 7. The ratio of buoyancy flux to sensible heat flux as a function of the ratio of latent to sensible heat flux (in W m^{-2}). The solid line is calculated for the mean observed surface conditions, $\bar{\theta} = 300$ K, $\bar{Q} = 0.01$ kg/kg. The zero crossing indicates the point at which heat and humidity flux contributions to the buoyancy flux balance. The error in θ_L resulting from the use of buoyancy flux in its definition is $w'\theta'_v/w'\theta' - 1$, indicated by the arrows. The observed values for the turbulence runs are indicated by circles (upwind) and triangles (downwind).

the difference in sign between these results and those of Shao and Hacker (1990) is a result of the sign convention used in the scaling variable and the direction of the flux (Shao and Hacker actually calculate σ_Q^2/Q_L^2 and thus values of ± 3 are equally valid). To maintain a consistent set of scale definitions we retain the factor of -1 in Q_L resulting in negative values of the scaled standard deviations, but for the purposes of comparison with other studies only the magnitude is of relevance. The uppermost values in each stack have the rather larger values of -4.17 and -5.64 and will be discussed below. The close grouping of the scaled values indicates that local similarity holds for these measurements, and that Q_L is an appropriate scaling variable. The turbulent velocity components are also seen to scale successfully.

Local similarity theory predicts that scaled variables should be functions only of z/L_L , and should approach constant values as $z/L_L \rightarrow \infty$. In practice many studies have found scaled variables to be nearly constant for $z/L_L > 0$. Thus for stable conditions scaled variables are expected to be independent of altitude and

the degree of stability, at least for $z/L_L \gg 1$. For unstable conditions, however, a stability dependence is expected. As conditions become increasingly convective the boundary layer becomes better mixed and local variations in scalar quantities such as temperature and humidity are smoothed out. Their standard deviations are thus expected to decrease; at the same time the vertical fluxes upon which the scaling variables are based may increase. σ_θ/θ_L and σ_Q/Q_L are thus expected to decrease. The local velocity scale is expected to decrease as buoyancy forcing dominates shear forcing and the scaled values of σ_u , σ_v , and σ_w will thus increase with increasingly unstable conditions. A number of parameterisations for this stability dependence have been proposed (Nieuwstadt, 1984; Sorbjan, 1986; Shao and Hacker, 1990). The small range in z/L_L observed in this study makes it difficult to draw firm conclusions about the behaviour of the scaled variables with stability; however, some general features can be related to previous results.

Figure 8 shows the scaled values of σ_w , σ_U , σ_θ , and σ_Q plotted against z/h . The approximate range of values from previous studies are indicated for comparison. Figure 9 shows the same values plotted as a function of z/L_L . The scaled standard deviations of temperature and humidity, though displaying significant scatter, show no coherent trend with either z/h or z/L_L . The values for temperature lie well within the range of previous observations, while those for humidity are slightly lower than the mean value found by Shao and Hacker (1990), but display substantially less scatter. The uppermost values for both temperature and humidity depart significantly from the values lower in the BL. This is due to a combination of the effects of entrainment and small changes in the relative position of the aircraft within the large vertical gradients of θ and Q at the top of the BL. Local similarity is not expected to apply within the entrainment zone (Sorbjan, 1986). The scaled values of σ_w and σ_U show a distinct increasing trend with altitude. This is due to the increase in z/L_L with altitude as the stability increases. Both σ_w/u_L and σ_U/u_L have a minimum at $z/L_L = 0$ and appear to increase towards values of approximately 1.4 and 4.2 respectively (neglecting the outlying maximum values at approximately 1.85 and 4.8). The outliers result from low values of u_L for the upwind run at 261 m. This flight leg lies just below a region of near uniform wind speed; the low shear means very little momentum is transported down and hence u_L has a small value. σ_w and σ_U do not exhibit a similar sudden drop in value but decrease approximately linearly with altitude. The behaviour of σ_w/u_L is in excellent agreement with that observed by Nieuwstadt (1984), who found a near constant value of 1.4 for $z/L_L > 1$, falling slightly to about 1.2 as z/L_L approached zero. The value approached by σ_U/u_L is larger than that observed previously. The reason for this is not clear but may be due to a larger fraction of the turbulent kinetic energy being associated with the horizontal wind components, possibly as a result of the higher wind speeds here compared to those in most of the earlier studies.

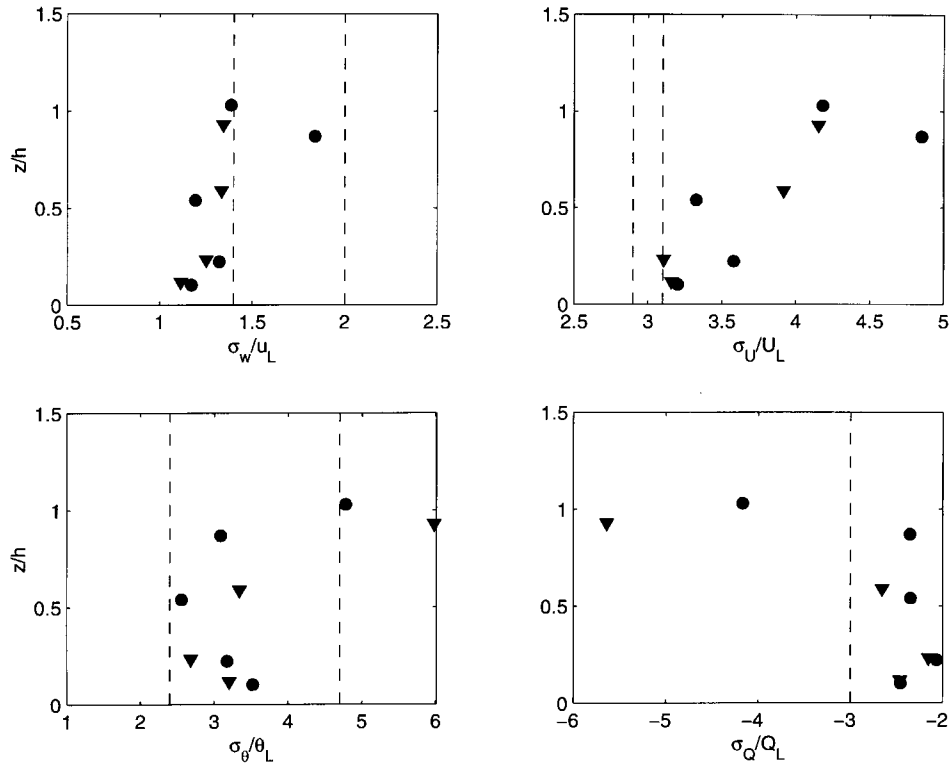


Figure 8. Scaled values of σ_w , σ_θ , σ_Q , and $\sigma_U = (\sigma_u^2 + \sigma_v^2)^{0.5}$ plotted against z/h for upwind (circles) and downwind (triangles) runs. Dashed lines indicate the range of mean values observed in previous studies.

5. Summary and Conclusions

Measurements over the central Persian Gulf have illustrated the mean and turbulent structure of a boundary layer during the late stages of its evolution from a stable internal boundary layer into a new marine atmospheric boundary layer. The observations were made during a winter shamal – a period of persistent hot, dry, high winds from the north of the Gulf. Wind speeds reached a maximum of about 23 m s^{-1} . The initial BL observed at the coast showed substantial modification by the surface. At the location of the aircraft observations the BL had reached near equilibrium with the surface, although some minor modification continued alongwind. Subsidence warming of the entire lower atmosphere over the Gulf offset the heat loss to the surface from the BL, and maintained a near constant sensible heat flux of about -15 W m^{-2} throughout the measurement region. A substantial upward latent heat flux was observed, having a magnitude of approximately 250 W m^{-2} at the upwind end of the observation region, falling to about 200 W m^{-2} downwind as the BL humidity increased. This exceptionally large humidity flux

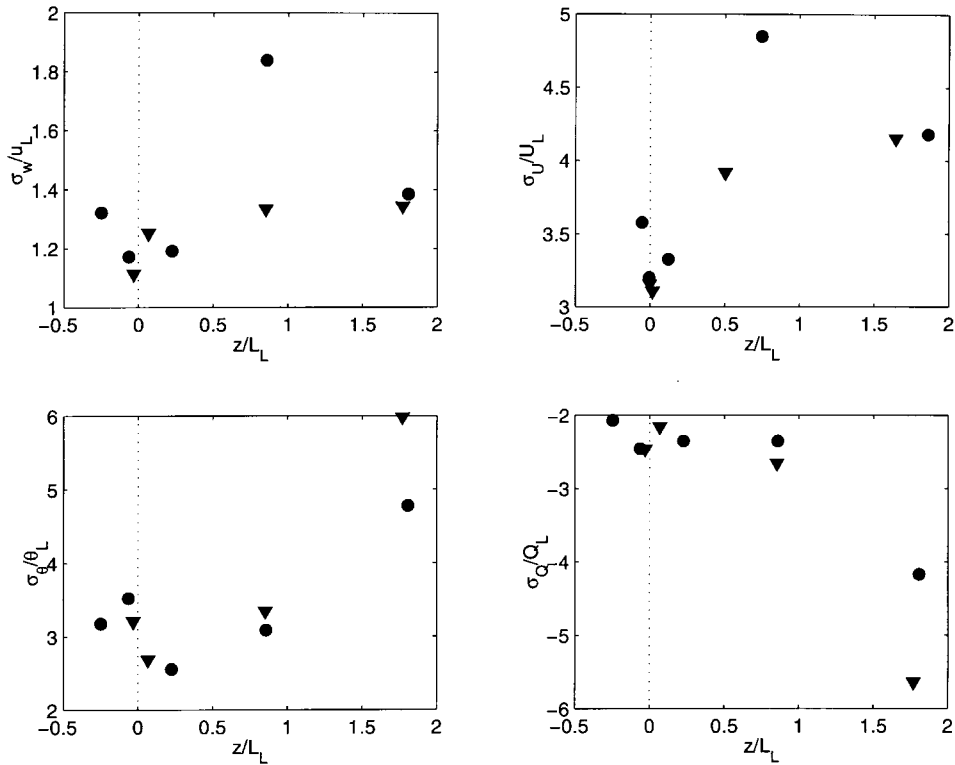


Figure 9. Scaled variables as in Figure 8, but plotted as functions of z/L_L .

was sufficient to overcome the downward heat flux and maintain weak buoyant convection in the lowest part of the BL. The buoyant forcing was, however, very weak over the region of aircraft observations, amounting to less than 2% of the shear contribution to the TKE budget. The depth of the convective layer decreased along-wind as the surface humidity flux decreased. Ogive curves of the sensible and latent heat contributions to the buoyancy flux also reveal that although the total heat flux is directed downwards, there is a small upward, counter-gradient heat flux at small scales (≤ 50 m). This counter-gradient flux is greatest near the surface, and is attributed to the break-up of larger eddies bringing warmer air down from higher levels and the subsequent return of fluid elements towards their level of neutral buoyancy.

Local similarity scaling was applied to the turbulence measurements. The standard deviations of temperature, humidity, and the wind speed components were all found to scale successfully. In general the scaled values are expected to be functions of z/L_L , and to approach constant values under stable conditions. The scaled temperature and humidity were found to be nearly constant in value, except at the top of the boundary layer where entrainment and large scale variability associated with the motion of the aircraft through the large vertical gradients at boundary

layer top cause the scaling to break down. σ_θ/θ_L had values well within the range observed by previous studies. There are few published results for humidity; those of Shao and Hacker display much greater scatter than observed here, though they centre about a similar value. Our observations of scaled wind velocities display the dependence on stability expected in the range $0 < z/L_L < 2$, approaching a constant value with increasing stability; σ_w/u_L shows excellent agreement with the results of Nieuwstadt (1984); σ_U/u_L has values rather larger than observed in previous studies, possibly due to differences in the partitioning of TKE between vertical and horizontal wind components between the different studies. Three of the flight legs include in this analysis were made within the shallow unstable layer near the surface. The very narrow range of z/L_L within the convective layer and small number of data points make it impossible to identify differing trends between the stable and unstable layers. In general the points from the unstable surface layer are grouped closely with those from the runs with weakest stability.

The combination of sensible and latent heat fluxes observed serve to emphasise an inconsistency in the customary definitions of the length and temperature scales. The length scale is a measure of the relative strength of the buoyant and mechanical forcing of the BL. It is defined to have the same sign as the Richardson number – positive in stable conditions, negative in unstable conditions. In common with many aspects of boundary-layer meteorology, local similarity theory was first developed and tested using data from studies conducted over land. Humidity was not a significant factor and buoyancy forcing was determined solely by the sensible heat flux. The length and temperature scales were thus defined in terms of the sensible heat flux. Over water surfaces, humidity becomes a significant factor in determining buoyancy. Static stability is dependant on θ_v rather than θ and so the buoyancy flux is substituted for heat flux in the definition of L_L . This definition is applicable to all conditions and approaches the value of the original definition as the humidity contribution to the buoyancy flux decreases. It has become common practice to define the temperature scale in terms of the buoyancy flux also. It is not clear why this has become the case; probably to maintain the relationship between θ_L and L_L established by the substitution of θ_L into the definition of the length scale, as shown in (2) and (3). Many standard texts simply define both L_L and θ_L directly in terms of the buoyancy flux (Stull, 1988; Garratt, 1992). The results of this study show that while L_L should clearly be defined in terms of the buoyancy flux, as in (3), θ_L should be defined in terms of the sensible heat flux, as in (2), and its substitution into the equation for L_L is not valid for the general case. In many cases the error resulting from the use of buoyancy flux in the definition of θ_L will not be obvious. When the magnitude of the latent heat flux is within a factor of two of the sensible heat flux, the error in θ_L is less than 15% and local scaling may appear to be satisfied. Also, if the ratio between sensible and latent heat fluxes remains constant, then local scaling will appear to apply, but the absolute value of the scaled temperature will be in error. Modest errors would likely be apparent only as an increase in the apparent variability. It is of interest to note that in the study

by Rogers et al. (1995) where θ_L is defined in terms of the buoyancy flux that the range of individual values of σ_θ/θ_L is double that in the present study (excluding data at or above BL top).

Acknowledgements

This work was supported by the Office of Naval Research Marine Meteorology Program and the U.K. Meteorological Office. We would like to express our gratitude to the Royal Air Force crew of the C-130 Hercules for their work during this project, and in particular Mr. Chris O'Brien (Officer in Charge) for his help co-ordinating the flights with the U.S. Navy.

References

- Brooks, I. M., Goroch, A. K., and Rogers, D. P.: 1999, 'Observations of Strong Surface Radar Ducts over the Persian Gulf', *J. Appl. Meteorol.* **38**, 1293–1310.
- Craig, R. A.: 1946, 'Measurements of Temperature and Humidity in the Lowest 1000 Feet of the Atmosphere over Massachusetts Bay', *Pap. Phys. Oceanogr. and Meteorol.* **10**, 1–46.
- Emmons, G.: 1947, 'Vertical Distributions of Temperature and Humidity over the Ocean between Nantucket and New Jersey', *Pap. Phys. Oceanogr. and Meteorol.* **10**(3), 1–89.
- Friehe, C. A., Shaw, W. J., Rogers, D. P., Davidson, K. L., Large, W. G., Stage, S. A., Crescenti, G. H., Khalsa, S. J. S., Greenhut, G. K., and Li, F.: 1991, 'Air-Sea Fluxes and Surface Layer Temperatures around a Sea-Surface Temperature Front', *J. Geophys. Res.* **96**, 8593–8609.
- Garratt, J. R.: 1987, 'The Stably Stratified Internal Boundary Layer for Steady and Diurnally Varying Offshore Flow', *Boundary-Layer Meteorol.* **38**, 369–394.
- Garratt, J. R.: 1990, 'The Internal Boundary Layer – A Review', *Boundary-Layer Meteorol.* **50**, 171–203.
- Garratt, J. R.: 1992, *The Atmospheric Boundary Layer*, Cambridge University Press, 316 pp.
- Garratt, J. R. and Ryan, B. F.: 1989, 'The Structure of the Stably Stratified Internal Boundary Layer in Offshore Flow over the Sea', *Boundary-Layer Meteorol.* **47**, 17–40.
- Hsu, S. A.: 1983, 'On the Growth of a Thermally Modified Boundary Layer by Advection of Warm Air over a Cooler Sea', *J. Geophys. Res.* **88**(C1), 771–774.
- Koracin, D. and Rogers, D. P.: 1990, 'Numerical Simulations of the Response of the Marine Atmosphere to Ocean Forcing', *J. Atmos. Sci.* **47**, 592–611.
- McCarthy, J.: 1973, 'A Method for Correcting Airborne Temperature Data for Sensor Response Time', *J. Appl. Meteorol.* **12**, 211–214.
- Melas, D.: 1989, 'The Temperature Structure in a Stably Stratified Internal Boundary Layer over a Cold Sea', *Boundary-Layer Meteorol.* **48**, 361–375.
- Mulhearn, P. J.: 1981, 'On the Formation of a Stably Stratified Internal Boundary-Layer by Advection of Warm Air over a Cooler Sea', *Boundary-Layer Meteorol.* **21**, 247–254.
- Nappo, C. J. and Bach, W. D.: 1997, 'Summary Report on the ARO/ARL Workshop on Turbulence and Diffusion in the Stable Planetary Boundary Layer', *Bull. Amer. Meteorol. Soc.* **78**, 493–498.
- Nicholls, S.: 1978, *An Observational Study of the Mid-Latitude, Marine Atmospheric Boundary Layer*, Ph.D. Thesis, University of Southampton, U.K.
- Nieuwstadt, F. T. M.: 1984, 'The Turbulent Structure of the Stable, Nocturnal Boundary Layer', *J. Atmos. Sci.* **41**, 2202–2216.

- Perrone, T. J.: 1979, 'Winter Shamal in the Persian Gulf', Naval Environmental Publication Research Facility, Monterey, CA., Report No. NEPRF-TR-7906, 180 pp.
- Rogers, D. P., 1989, 'The Marine Boundary Layer in the Vicinity of an Ocean Front', *J. Atmos. Sci.* **46**, 2044–2062.
- Rogers, D. P.: 1995, 'Coastal Meteorology', *Rev. Geophys., Supplement, U.S. National Report to International Union of Geodesy and Geophysics*, pp. 889–895.
- Rogers, D. P., Johnson, D. W., and Friehe, C. A.: 1995a, 'The Stable Internal Boundary Layer over a Coastal Sea. I: Airborne Measurements of the Mean and Turbulence Structure', *J. Atmos. Sci.* **52**, 667–683.
- Rogers, D. P., Johnson, D. W., and Friehe, C. A.: 1995b, 'The Stable Internal Boundary Layer over a Coastal Sea. II: Gravity Waves and the Momentum Balance', *J. Atmos. Sci.* **52**, 684–696.
- Shao, Y. and Hacker, J. M.: 1990, 'Local Similarity Relationships in a Horizontally Inhomogeneous Boundary Layer', *Boundary-Layer Meteorol.* **52**, 17–40.
- Smedman, A.-S., Bergström, H., and Grisogono, B.: 1997, 'Evolution of Stable Internal Boundary Layers over a Cold Sea', *J. Geophys. Res.* **102**(C1), 1091–1099.
- Sorbjan, Z.: 1986, 'On Similarity in the Atmospheric Boundary Layer', *Boundary-Layer Meteorol.* **34**, 377–397.
- Sorbjan, Z.: 1987, 'An Examination of the Local Similarity Theory in the Stably Stratified Boundary Layer', *Boundary-Layer Meteorol.* **38**, 63–71.
- Stull, R. B.: 1988, *An Introduction to Boundary-Layer Meteorology*, Kluwer Academic Publishers, Dordrecht, 666 pp.
- Tjernström, M. and Smedman, A.-S.: 1993, 'The Vertical Turbulence Structure of the Coastal Marine Atmospheric Boundary Layer', *J. Geophys. Res.* **98**(C3), 4809–4826.